Available online at www.sciencedirect.com
ScienceDirect
Biomedical Signal Processing and Control 3 (2008) 29–43
Biomedical Signal Processing and Control
www.elsevier.com/locate/bspc

A dynamic model to characterize beat-to-beat adaptation of repolarization to heart rate changes

Esther Pueyo [a,*], Marek Malik [b], Pablo Laguna [a]

[a] Communications Technology Group (GTC) at the Aragón Institute for Engineering Research (I3A), CIBER-BBN, University of Zaragoza, 50018 Zaragoza, Spain
[b] Department of Cardiological Sciences, St. George's Hospital Medical School, SW17 ORE London, United Kingdom

Received 30 January 2007; received in revised form 24 August 2007; accepted 18 September 2007

Abstract

An adaptive approach is presented to investigate, on a beat-to-beat basis, the response to heart rate variations of the QT interval and the *T* wave amplitude (T_a). The relationship between each repolarization index and the RR interval is modeled using a time-variant system composed of a linear filter followed by a memoryless nonlinearity approximated by a Taylor expansion. The linear portion describes the influence of previous RR intervals on the repolarization index and the nonlinear portion expresses how the index evolves as a function of the averaged RR measurement ($\overline{RR}$) at the output of the linear filter. For the identification of the unknown system, two procedures that simultaneously estimate all of the system parameters are proposed. The first procedure converts the total input–output relationship into one being linear in its parameters and uses a Kalman-based technique to estimate these parameters. The second procedure uses the Unscented Kalman Filter to solve the nonlinear identification directly. Those procedures were tested on artificially generated data and showed very good agreement between estimated and theoretical parameter values. The application to electrocardiographic recordings showed that both repolarization indices lag behind the RR interval, being the effect more noticeable for the QT interval and more strongly manifested in episodes of sustained changes in heart rate, with QT lags after large RR variations of nearly 1 min in mean over recordings. The time variant $QT/\overline{RR}$ relationship was found to be adequately modeled by a first-order Taylor expansion, while the $T_a/\overline{RR}$ relationship was better modeled using a second-order nonlinearity.

Keywords: QT adaptation; QT/RR relationship; Nonlinear models

1. Introduction

Since the extensive reports showing that impaired adaptation of the QT interval to changes in heart rate (HR) might be associated with the risk of cardiac arrhythmias [1–3], the QT interval, which expresses the overall duration of ventricular depolarization plus repolarization, is one of the most well-studied indices of the surface electrocardiogram (ECG). Many of the studies that analyzed the relationship between QT and RR (the inverse of heart rate) were restricted to episodes in which the RR signal was stable [4], when the QT interval is affected mainly by the preceding RR interval. In situations where there is a large variation in cardiac rhythm, the influence of the history of preceding RR intervals on each QT measurement needs to be considered to account for the well-known hysteresis effect present in the QT/RR relationship [5–8]. In [5] a method was proposed to assess the QT interval response to changes in heart rate on ambulatory recordings and characteristics of the adaptation in terms of duration and profile were provided for individual recordings and for selected segments of the recording that showed abrupt changes in heart rate. Those characteristics were used to discriminate between post-myocardial infarction patients at high and low risk of arrhythmic death while on treatment with amiodarone. With that type of method, however, it is not possible to evaluate the QT dynamic behaviour on a beat-to-beat basis, which can be very useful in identifying instances when disturbances in the adaptation occur and which, on the other hand, can be masked by the static analysis performed in [5] if the overall adaptation is not modified. In this study, we develop and test a full beat-to-beat adaptation analysis that can describe changes in the QT

* Corresponding author.
E-mail addresses: epueyo@unizar.es (E. Pueyo), m.malik@sghms.ac.uk (M. Malik), laguna@unizar.es (P. Laguna).

1746-8094/$ – see front matter © 2007 Elsevier Ltd. All rights reserved.
doi:10.1016/j.bspc.2007.09.005

interval dynamically and relate them to variations in heart rate. Also, the index T_a measuring the T wave amplitude is examined, which has been shown to have a strong heart rate dependence [9]. Since recent works published in the literature have documented that assessment of T wave morphology changes in relation to heart rate can provide more insight into repolarization abnormalities [9,10], we have also investigated in this study the beat-to-beat adaptation of T_a in response to rate variations, using the same methodology as for the QT interval.

To perform the investigation, we propose a general model that, when applied to ECG data, takes the RR series, after interpolation, as the input signal $x_{RR}(n)$ and the corresponding interpolated QT series as the output signal $y_{QT}(n)$, where n is the discrete time index. Analogously, the analysis is performed taking as output signal the interpolated T_a series, $y_{T_a}(n)$. In the description of the methods, the output signal will be generically denoted by $y_{QT}(n)$ to simplify the reading. The system proposed in this study to relate the input and output signals $x_{RR}(n)$ and $y_{QT}(n)$ is assumed to be composed of a linear time-variant FIR filter followed by a zero-memory nonlinear function represented by a Pth-order Taylor polynomial ($P > 0$) whose coefficients are permitted to vary over time. Since the underlying system is time-varying and the stochastic process that supplies the tap inputs can be nonstationary (e.g., in the analysis of the QT/RR or T_a/RR relationship in ambulatory recordings), the adaptive filter proposed for system identification has to deal with nonstationary environments. This led us to formulate the problem using state-space models and apply Kalman-based filters to solve it.

The proposed methodology was evaluated using simulated data and, subsequently, applied to the analysis of real ECG recordings to assess the QT/RR and T_a/RR adaptation on a beat-to-beat basis. ECG data were obtained from healthy subjects as they changed their posture in a prescribed way, which caused substantial and, frequently, very abrupt changes in heart rate. In this study, we investigated the mode of adaptation of the two repolarization indices to those changes in rate and we explored interindividual differences. Also, we examined differences in the adaptation to accelerating and decelerating heart rates.

The paper is organized as follows: Section 2 contains the procedures of the study, and the data are described in Section 3. Section 4 proposes a number of performance measures for assessing the procedure. Section 5 presents the results, which are discussed in Section 6.

2. Methods

2.1. Model composition

A nonlinear system with memory is used to model the relationship between scalar and real input and output signals, $x_{RR}(n)$ and $y_{QT}(n)$, respectively. The input signal $x_{RR}(n)$ is the realization of a stochastic process that can be nonstationary and for which no a priori probability density function distribution is assumed. In the ECG application, the input $x_{RR}(n)$ represents an RR interval series interpolated to a sampling rate of 1 Hz, while the output $y_{QT}(n)$ corresponds to a 1 Hz-interpolated QT interval series. The system to be identified (Fig. 1) is assumed to be composed of a linear time-variant FIR filter of order N:

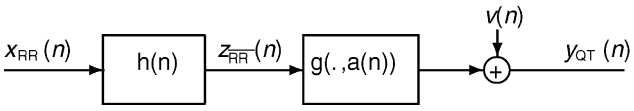

Fig. 1. Block structure of the system used in the study, which is composed of a linear FIR time-variant filter h(n) followed by a time-varying nonlinear function $g(\cdot, \mathbf{a}(n))$. The output of the system is corrupted by additive noise $v(n)$.

$$\mathbf{h}(n) = [h_0(n), \ldots, h_{N-1}(n)]^{\mathrm{T}} \in \mathbb{R}^{N\times 1}, \tag{1}$$

whose output is denoted by $z_{\overline{RR}}(n)$, followed by a time-varying zero-memory nonlinearity $g(\cdot)$ that is expandable as a Pth-order Taylor series around a bias point:

$$g(z_{\overline{RR}}(n), \mathbf{a}(n)) = \sum_{k=0}^{P} a_k(n) z_{\overline{RR}}^{k}(n), \tag{2}$$

with $\mathbf{a}(n) = [a_0(n), \ldots, a_P(n)]^{\mathrm{T}} \in \mathbb{R}^{(P+1)\times 1}$. The Taylor expansion for the nonlinearity $g(\cdot)$ is valid in a neighbourhood of a bias point different from 0 and the original Taylor series was subsequently reformulated as in Eq. (2), with the bias point integrated in the coefficients. The orders N and P of the subsystems are defined a priori based on the characteristics of the input and output signals to be processed. In the case of the QT/RR relationship, it is sufficient to consider polynomial nonlinearities up to order $P = 2$ and filter lengths up to $N = 50$ (which corresponds to 50 s due to series interpolation to 1 Hz) because even a larger number of preceding RR intervals can influence each QT, the initial 40–50 s are the most clinically relevant [5].

An important remark about the identification of the proposed system is that its linear and nonlinear portions can only be determined up to a scale factor, because the multiplication of each filter weight by a factor η (i.e., $\eta h_i(n)$, $i = 0, \ldots, N-1$) and the division of the nonlinearity coefficients by η^k (i.e., $a_k(n)/\eta^k$, $k = 0, \ldots, P$) does not alter the output of the overall system. If a restriction is imposed on the linear filter, such as $\mathbf{h}^T(n)\mathbf{1} = 1, \forall n$, with $\mathbf{1}$ denoting the $N \times 1$ vector of ones, uniqueness in the estimation of the filter weights and nonlinearity coefficients is guaranteed. Other constraints are imposed in the identification procedure with the objective of providing a meaningful physiological interpretation of the ventricular repolarization adaptation. The constraints are such that all of the filter weights in $\mathbf{h}(n)$ are positive, which permits the interpretation of the relative contribution of previous RR intervals to each QT measurement.

With such restrictions, the output of the linear portion,

$$z_{\overline{RR}}(n) = \mathbf{h}^{\mathrm{T}}(n)\mathbf{x}_{RR}(n), \tag{3}$$

where

$$\mathbf{x}_{RR}(n) = [x_{RR}(n)\, x_{RR}(n-1) \ldots x_{RR}(n-N+1)]^{\mathrm{T}}, \tag{4}$$

can be interpreted in the ECG application as a running weighted-averaged RR measurement with weights specifically defined at each instant n. The nonlinear subsystem is representative of how

the QT interval (global output signal $y_{QT}(n)$) evolves as a function of such an averaged RR measurement ($z_{\overline{RR}}(n)$).

The output of the unknown system is assumed to be corrupted by additive white noise $v(n)$ that is uncorrelated with the input $x_{RR}(n)$. The noise signal $v(n)$ can include, for instance, delineation errors generated in the determination of the QT interval and terms in $y_{QT}(n)$ that are not well represented by the assumed model. Consequently, the output of the global system can be written as

$$y_{QT}(n) = g(z_{\overline{RR}}(n), \quad \mathbf{a}(n)) + v(n) = \mathbf{a}^{T}(n)\mathbf{z}_{\overline{RR}}(n) + v(n), \tag{5}$$

where

$$\mathbf{z}_{\overline{RR}}(n) = [1 z_{\overline{RR}}(n) \dots z^{P}_{\overline{RR}}(n)]^{T}. \tag{6}$$

2.2. Adaptive estimation of model parameters

Given the input and output signals $x_{RR}(n)$ and $y_{QT}(n)$, the simultaneous estimation of the system parameters (i.e., $\mathbf{h}(n)$ and $\mathbf{a}(n)$) is confronted using two different approaches, which are described in the following.

2.2.1. Volterra Linearized–Kalman Filter approach (VL–KF)

The VL–KF technique uses an adaptive linear filter to identify the global time-variant system at each time instant. To that end, the Taylor series expansion that approximates the nonlinearity is converted into a relationship that allows the output of the unknown system to be expressed as a linear combination of known functions of the input signal, and the Kalman Filter (KF) is used to estimate the coefficients of the combination. This is performed as follows.

2.2.1.1. Volterra series expansion. According to the model structure considered in this study, described in Section 2.1, the output $y_{QT}(n)$ is expressed as:

$$\begin{aligned} y_{QT}(n) &= g(z_{\overline{RR}}(n), \mathbf{a}(n)) + v(n) \\ &= \sum_{k=0}^{P} a_k(n) \left(\sum_{i=0}^{N-1} h_i(n) x_{RR}(n-i) \right)^{k} + v(n). \end{aligned} \tag{7}$$

Denoting

$$m_0(n) = a_0(n) \tag{8}$$

$$m_k(i_1, i_2, \dots, i_k; \ n) = \frac{k!}{\prod_{q=0}^{N-1} l_q(i_1, i_2, \dots, i_k)!} a_k(n) \prod_{j=1}^{k} h_{i_j}(n), \quad k = 1, \dots, P, \tag{9}$$

where $l_q(i_1, i_2, \dots, i_k)$ counts the number of indexes in $\{i_1, i_2, \dots, i_k\}$ that are equal to q, $q \in \{0, \dots, N-1\}$, the expression above for $g(z_{\overline{RR}}(n), \mathbf{a}(n))$ can be transformed into one that is linear in its parameters:

$$\begin{aligned} &g(z_{\overline{RR}}(n), \ \mathbf{a}(n)) \\ &\quad = m_0(n) \\ &\qquad + \sum_{k=1}^{P} \sum_{i_1=0}^{N-1} \sum_{i_2=i_1}^{N-1} \cdots \sum_{i_k=i_{k-1}}^{N-1} m_k(i_1, i_2, \dots, i_k; \ n) \prod_{j=1}^{k} x_{RR}(n-i_j). \end{aligned} \tag{10}$$

Furthermore, the following notations are introduced:

$$\mathbf{m}(n) = [\mathbf{m}_0^{T}(n) \, \mathbf{m}_1^{T}(n), \dots, \mathbf{m}_P^{T}(n)]^{T}, \tag{11}$$

$$\mathbf{m}_0(n) = m_0(n) \tag{12}$$

$$\begin{aligned} \mathbf{m}_k(n) = [&m_k(0, \dots, 0, 0; \ n), \dots, m_k(i_1, \dots, i_j, \dots, i_k; \ n), \dots, \\ &m_k(N-1, \dots, N-1, N-1; \ n)]^{T}, \quad i_j \geq i_{j-1}, \\ &1 \leq k \leq P, \end{aligned} \tag{13}$$

and

$$\mathbf{s}(n) = [\mathbf{s}_0^{T}(n) \, \mathbf{s}_1^{T}(n), \dots, \mathbf{s}_P^{T}(n)]^{T}, \tag{14}$$

$$\mathbf{s}_0(n) = 1 \tag{15}$$

$$\mathbf{s}_k(n) = \left[x^{k}_{RR}(n), \dots, \prod_{j=1}^{k} x_{RR}(n-i_j), \dots, x^{k}_{RR}(n-N+1)\right]^{T}, \quad i_j \geq i_{j-1}, \quad 1 \leq k \leq P. \tag{16}$$

With those notations, the output of the global system can be expressed in vector form as

$$y_{QT}(n) = \mathbf{s}^{T}(n)\mathbf{m}(n) + v(n), \tag{17}$$

where $\mathbf{s}(n)$ is the known observation vector and $\mathbf{m}(n)$ is the parameter vector to be estimated. Both $\mathbf{s}(n)$ and $\mathbf{m}(n)$ are vectors of size $L_{\mathbf{m}} \times 1$, with

$$L_{\mathbf{m}} = \sum_{j=0}^{P} f_{CR}(N, j) = \left(\frac{N+P}{N} \right), \tag{18}$$

where f_{CR} (N, j) denotes the number of all of the possible combinations with repetition of a set of N different elements in subsets of length j, and $\left(\frac{N+P}{N}\right)$ is the combinatorial of $N+P$ over N.

2.2.1.2. State-space formulation. The underlying model, in the form expressed after the linearization procedure is applied, now is formulated as a state-space representation (see [11], p. 470) that includes, apart from the observation Eq. (17), a description of the time-varying nature of the quantities to be estimated.

In that way, the proposed finite-dimensional linear state-space model for the output process $y_{QT}(n)$ is defined by the following pair of equations: the *measurement equation*, which expresses $y_{QT}(n)$ as

$$y_{QT}(n) = \mathbf{s}^{T}(n) \, \mathbf{m}(n) + v(n), \quad n \geq 0, \tag{19}$$

where $\mathbf{m}(n)$ is the *state-vector* and $v(n)$ is the *measurement noise*; on the other hand, the *process equation*, which describes

the recursion that the state-vector obeys as

$$\mathbf{m}(n+1) = \mathbf{F}(n)\,\mathbf{m}(n) + \mathbf{u}_{\mathbf{m}}(n), \quad n \geq 0, \tag{20}$$

where $\mathbf{u}_{\mathbf{m}}(n)$ is the *process noise*. Here, a random-walk model [11] is used in the process equation ($\mathbf{F}(n) = \mathbf{I}$, where $\mathbf{I}$ is the identity matrix).

The processes $v(n)$ and $\mathbf{u}_{\mathbf{m}}(n)$ are assumed to be zero-mean white noise processes. The variance of $v(n)$ is denoted by $\sigma_v^2(n)$, while the covariance of $\mathbf{u}_{\mathbf{m}}(n)$ is denoted by $\mathbf{Q}_{\mathbf{u_m}}(n)$. Unless there is feedback from the output to the states, those noises can be assumed to be uncorrelated, as it is the case for our purposes. The initial state $\mathbf{m}(0)$ is assumed to be a random vector with mean $\boldsymbol{\mu}_{0,\mathbf{m}}$ and covariance matrix $\Pi_{0,\mathbf{m}}$, and uncorrelated with $v(n)$ and $\mathbf{u}_{\mathbf{m}}(n)$. In our implementation of the Kalman Filter, the mean of the state estimate at time $n = 0$ is assigned a value $\boldsymbol{\mu}_{0,\mathbf{m}}$ that is built up using the expressions (8), (9) and (11)–(13) and vectors $\boldsymbol{\mu}_{0,\mathbf{h}}$ and $\boldsymbol{\mu}_{0,\mathbf{a}}$, which are defined as follows: $\boldsymbol{\mu}_{0,\mathbf{h}}$ is taken to be a normalized exponentially decreasing weight curve of factor $\alpha(0)$, with $\alpha(0)$ determined from a set of possible values in the interval [0,1] as the one leading to minimum residuum of the Pth-order polynomial fit between $y_{\mathrm{QT}}(n)$ and $z_{\overline{\mathrm{RR}}}(n)$, for $n = 0, \ldots, 99$, and $z_{\overline{\mathrm{RR}}}(n)$ calculated using $\alpha(0)$; on the other hand, $\boldsymbol{\mu}_{0,\mathbf{a}}$ is obtained by optimally fitting the $[y_{\mathrm{QT}}(n),\ z_{\overline{\mathrm{RR}}}(n)]$ data of the initial 100 samples with a polynomial of order P, where $z_{\overline{\mathrm{RR}}}(n)$ is defined using the vector $\boldsymbol{\mu}_{0,\mathbf{h}}$ just described. The initial covariance matrix $\Pi_{0,\mathbf{m}}$ is taken as the identity matrix. The initializations $\boldsymbol{\mu}_{0,\mathbf{m}}$ and $\Pi_{0,\mathbf{m}}$ have an effect only at the beginning of the estimation, but plausible values are chosen for consistency. In the application of the Kalman Filter it is generally assumed that the matrices $\mathbf{s}(n)$, $\mathbf{Q}_{\mathbf{u_m}}(n)$, $\sigma_v^2(n)$ and $\Pi_{0,\mathbf{m}}$ are known a priori. For our problem, the matrices $\mathbf{Q}_{\mathbf{u_m}}(n)$ and $\sigma_v^2(n)$ are not known and need to be estimated (see below).

2.2.1.3. Regularization. Before we apply the Kalman Filter to solve the linear state-space problem for the unknown vector $\mathbf{m}(n)$, note the ill-posing of the formulated problem. To this point, the state vector $\mathbf{m}(n)$ would be calculated using a noisy observation $y_{\mathrm{QT}}(n)$, only, if the Kalman Filter without regularization is used, which can lead to inaccurate estimates. To improve the estimation, a regularization process is incorporated that reduces greatly the effect of small noise perturbations in the output signal affecting the state estimates. The fundamental idea behind regularization is the addition of extra relationships on the parameters to be estimated based on a priori knowledge about them. For our application, it is reasonable to assume that the curve drawn by the vector $\mathbf{h}(n)$ expressing QT dependence on previous RR intervals is smooth, so that unexpected sharp spikes are avoided. In this study, such a condition is approximately satisfied by defining a regularization term that induces an exponential shape for $\mathbf{h}(n)$, which is justified according to [5]. The regularization process is performed using a time-varying extension of the Tikhonov-type regularization [12]. The approach considers the state-space problem, which is formulated in this study in the Eqs. (19) and (20), and augments the problem based on prior information about the state vector $\mathbf{m}(n)$ represented through a linear operator $\Phi(n)$. The new state-space problem has the same process equation as the previous one, but its measurement equation is as follows:

$$\tilde{\mathbf{y}}_{\mathrm{QT}}(n) = \tilde{\mathbf{S}}^{\mathrm{T}}(n)\,\mathbf{m}(n) + \tilde{\mathbf{v}}(n), \tag{21}$$

where

$$\tilde{\mathbf{y}}_{\mathrm{QT}}(n) = \begin{bmatrix} y_{\mathrm{QT}}(n) \\ \varphi(n) \end{bmatrix}, \quad \tilde{\mathbf{S}}(n) = \begin{bmatrix} \mathbf{s}^{\mathrm{T}}(n) \\ \Phi(n) \end{bmatrix}^{\mathrm{T}} \quad \text{and}$$

$$\tilde{\mathbf{v}}(n) = \begin{bmatrix} v(n) \\ \mathbf{v}'(n) \end{bmatrix}. \tag{22}$$

In this study, the vector $\varphi(n)$ is the null column vector of dimension $N^P \times 1$: $\varphi(n) = \mathbf{0}$.

The transformation $\boldsymbol{\Phi}(n)$, of dimension $N^P \times L_{\mathbf{m}}$, is computed in separate blocks affecting $\mathbf{m}_0(n), \ldots, \mathbf{m}_P(n)$:

$$\Phi(n) = \beta(n)\,\mathbf{D}(n), \tag{23}$$

where $\beta(n)$ is a parameter that controls the degree of smoothness of the estimates and $\mathbf{D}(n)$ is the matrix defined as

$$\mathbf{D}(n) = \begin{bmatrix} \mathbf{D^0}(n) & \mathbf{0} & \cdots & \mathbf{0} \\ \mathbf{0} & \mathbf{D^1}(n) & \cdots & \mathbf{0} \\ & & \ddots & \\ \mathbf{0} & \mathbf{0} & \mathbf{0} & \mathbf{D^P}(n) \end{bmatrix}. \tag{24}$$

The purpose of choosing that structure for matrix $\mathbf{D}(n)$ is to force the estimates in $\mathbf{m}(n)$ to satisfy the following:

$$\mathbf{D^k}(n)\,\mathbf{m}_k(n) = \mathbf{0}, \quad k = 0, \ldots, P. \tag{25}$$

The block $\mathbf{D^0}(n)$ is a scalar defined as 0 because no condition is required for $\mathbf{m}_0(n)$ (=$a_0(n)$).

The block $\mathbf{D^1}(n)$ is characterized by the following $(N-1) \times N$ matrix:

$$\mathbf{D^1}(n) = \begin{bmatrix} \alpha(n) & -1 & 0 & 0 & \cdots & 0 & 0 & 0 \\ 0 & \alpha(n) & -1 & 0 & \cdots & 0 & 0 & 0 \\ \vdots & & & & \ddots & & & \\ 0 & 0 & 0 & 0 & \cdots & 0 & \alpha(n) & -1 \end{bmatrix}, \tag{26}$$

which imposes an exponential relationship on the weight vector $\mathbf{h}(n)$ by forcing $\alpha(n)h_i(n) = h_{i+1}(n)$. The factor $\alpha(n)$ is determined, at each iteration of the Kalman Filter, using the available a priori estimate $\hat{\mathbf{m}}^-(n)$ (see Appendix A), from which the corresponding estimate $\hat{\mathbf{h}}^-(n)$ is readily derived. The normalization condition $(\hat{\mathbf{h}}^-(n))^{\mathrm{T}}\ \mathbf{1} = 1$, together with the imposition of exponential decay for $\hat{\mathbf{h}}^-(n)$, leads to:

$$\hat{h}_i^-(n \approx k(n)\alpha^i(n), \quad i = 0, \ldots, N-1, \tag{27}$$

with

$$\kappa(n) = \frac{1}{\sum_{i=0}^{N-1} \alpha^i(n)} = \frac{1-\alpha(n)}{1-\alpha^N(n)}, \tag{28}$$

being $\alpha(n)$ the factor that wants to be determined. Since all the weights $\hat{h}_i^-(n)$ are positive (this is one of the constraints incorporated into the estimation, as it will be described below),

the following approximation holds for large N:

$$\alpha(n) \approx 1 - \left(\max_{0\le i\le N-1}\{\hat{h}_i^-(n)\} - \min_{0\le i\le N-1}\{\hat{h}_i^-(n)\}\right). \quad (29)$$

For small N, $\alpha(n)$ is estimated as the mean of the quotients between consecutive elements of vector $\hat{\mathbf{h}}^-(n)$.

The block $\mathbf{D^2}(n)$ imposes constraints on the elements of $\mathbf{m}_2(n)$ equivalent to those imposed on the elements of $\mathbf{m}_1(n)$ through $\mathbf{D^1}(n)$. That block $\mathbf{D^2}(n)$ is derived by multiplying the entire set of relationships established in $\mathbf{D^1}(n)$ by each of the elements $h_0(n), \ldots, h_{N-1}(n)$, thereby obtaining $\mathbf{D^2}(n)$ as the matrix that has the following entries:

$$D^2_{ij}(n) = \left\{ \begin{array}{rl} \psi_{ij} D^1_{p_i \Omega_{ij}}(n), & \text{if } \Omega_{ij} \neq 0 \\ 0, & \text{if } \Omega_{ij} = 0 \end{array} \right\},$$
$$i = 1, \ldots, N(N-1), \quad j = 1, \ldots, f_{\mathrm{CR}}(N,2). \quad (30)$$

Elements p_i of vector $\mathbf{p}$ are defined as follows:

$$p_i = \left[\frac{i-1}{N}\right] + 1, \quad i = 1, \ldots, N(N-1), \quad (31)$$

where $[\cdot]$ denotes the integer part function. For the definition of the matrices Ω and Ψ in Eq. (30), the following notation is introduced: $\sigma_j\ \tau_j$ is the 1×2 vector that represents the j-th row of the matrix whose rows are the various combinations with repetition that can be taken of the elements of vector $[1, \ldots, N]$ in subsets of length 2. Those combinations are sorted in ascending order for σ_j first and then for τ_j. Then, the matrix Ω is recursively defined as

$$\Omega_{ij} = \left\{ \begin{array}{c} 1 + \sum_{l=1}^{j-1} b(\Omega_{il}), \\ 0, \end{array} \begin{array}{c} \left\{ \begin{array}{l} \text{if } (i-1)(\mathrm{mod}\ N) + 1 = \sigma_j \\ \text{or } (i-1)(\mathrm{mod}\ N) + 1 = \tau_j \end{array} \right\} \\ \text{otherwise} \end{array} \right\}, \ i$$
$$= 1, \ldots, N(N-1), \ j = 1, \ldots, f_{\mathrm{CR}}(N,2), \quad (32)$$

where $b : \mathbb{Z} \to \mathbb{Z}$ is defined as

$$b(t) = \left\{ \begin{array}{ll} 1, & \text{if } t \neq 0 \\ 0, & \text{if } t = 0 \end{array} \right., \quad t \in \mathbb{Z}. \quad (33)$$

Finally,

$$\Psi_{ij} = \left\{ \begin{array}{ll} 2, & \text{if } (i-1)(\mathrm{mod}\, N) + 1 = \Omega_{ij} \\ 1, & \text{otherwise} \end{array} \right\},$$
$$i = 1, \ldots, N(N-1), \quad j = 1, \ldots, f_{\mathrm{CR}}(N,2). \quad (34)$$

For nonlinearities of order P higher than 2, constructions analogous to that of $\mathbf{D^2}(n)$ lead to definitions of $\mathbf{D^3}(n)$, $\mathbf{D^4}(n)$, ..., which are the result of multiplying the conditions in the previous block by each of the elements $h_0(n), \ldots, h_{N-1}(n)$.

In the expression (23), the factor $\beta(n)$ is a positive scalar called the regularization parameter. The larger the regularization factor $\beta(n)$, the more strength is put into the smoothing; however, the selection of the factor is always a compromise because too large a value might lead to overregularized solutions that are not close to the true state vector $\mathbf{m}(n)$. In this study, $\beta(n)$ is identified using the *L-curve* criterion [13], that is, it is chosen as the optimum value that results from taking the associated $\hat{\mathbf{m}}(n)$ that yields the corner closest to (0,0) in the log–log plot of $||\mathbf{D}(n)\,\hat{\mathbf{m}}(n)||$ versus $||y_{\mathrm{QT}}(n) - \mathbf{s}(n)^{\mathrm{T}}\,\hat{\mathbf{m}}(n)||$, where $\hat{\mathbf{m}}(n)$ is the regularized a posteriori estimate of $\mathbf{m}(n)$ (see Appendix A). In that way, a good balance is achieved between the minimization of the perturbation error and the regularization error (see [13] for details).

Lastly, in Eq. (22), $\mathbf{v}'(n)$ is a fictitious zero-mean noise process that is uncorrelated with $\mathbf{m}(n)$ and $v(n)$ and has diagonal covariance matrix $\mathbf{R}_{\mathbf{v}'}(n)$ which, for our purposes, is chosen as the identity matrix. Consequently, the covariance of the augmented noise vector $\tilde{\mathbf{v}}(n)$ is

$$\mathbf{R}_{\tilde{\mathbf{v}}}(n) = \begin{bmatrix} \sigma_v^2(n) & \mathbf{0} \\ \mathbf{0} & \mathbf{I} \end{bmatrix}. \quad (35)$$

2.2.1.4. Kalman Filter. For the formulated linear state-space model (defined by Eqs. (20) and (21)), the Kalman Filter is used to solve optimally (minimum mean-square estimation error) the process and measurement equations for the unknown state vector $\mathbf{m}(n)$, which can be viewed as the minimum set of data sufficient to describe the system behaviour [11]. In our study, we used the time- and measurement-update form, which is one of the many possible implementations of the Kalman Filter. In that form, the computations can be grouped into two main blocks. One block contains the time-update equations (or "*projection equations*") in which the current state estimate and error covariance estimate are projected in time according to the process equation and produce a priori estimates for the next time step. The second block contains the measurement-update equations (or "*correction equations*"), which provide improved a posteriori estimates by incorporating information about the observed output into the a priori estimates. The time- and measurement-update blocks are run recursively, which leads to an estimate $\hat{\mathbf{m}}(n)$ of the state vector $\mathbf{m}(n)$ at each time instant n (see Appendix A).

2.2.1.5. Estimation of noise covariances. The matrices $\mathbf{Q}_{\mathbf{u_m}}(n)$ and $\sigma_v^2(n)$ need to be estimated at each iteration of the Kalman Filter. To that end, definition of the autocorrelation $\mathbf{R_m}(n) = E\{\mathbf{m}(n)\mathbf{m}^{\mathrm{T}}(n)\}$ of the unknown system response $\mathbf{m}(n)$ is considered. A straightforward procedure is used to generate estimates of $\mathbf{Q}_{\mathbf{u_m}}(n)$ and $\sigma_v^2(n)$. That procedure is a generalization of the method proposed in [14] and, now, extended to deal with the more general case of time-variant model matrices.

The inference of the covariance matrix $\mathbf{Q}_{\mathbf{u_m}}(n)$ of the process noise is obtained by premultiplying the transpose of the equation process by $\mathbf{m}(n+1)$, which leads to

$$\mathbf{m}(n+1)\,\mathbf{m}^{\mathrm{T}}(n+1) = \mathbf{m}(n+1)\,\mathbf{m}^{\mathrm{T}}(n) + \mathbf{m}(n+1)\,\mathbf{u}_{\mathbf{m}}^{\mathrm{T}}(n), \quad (36)$$

or, equivalently,

$$\mathbf{m}(n+1)\,\mathbf{m}^{\mathrm{T}}(n+1) = \mathbf{m}(n)\,\mathbf{m}^{\mathrm{T}}(n) + \mathbf{u_m}(n)\,\mathbf{m}^{\mathrm{T}}(n) + \mathbf{m}(n)\,\mathbf{u}_{\mathbf{m}}^{\mathrm{T}}(n) + \mathbf{u}_{\mathbf{m}}(n)\,\mathbf{u}_{\mathbf{m}}^{\mathrm{T}}(n). \quad (37)$$

Taking expectations and accounting for the uncorrelatedness of $\mathbf{m}(n)$ and $\mathbf{u}_{\mathbf{m}}(n)$ (which is easily derived from the assumptions on the model), we obtain:

$$\mathbf{R}_{\mathbf{m}}(n+1) = \mathbf{R}_{\mathbf{m}}(n) + \mathbf{Q}_{\mathbf{u}_{\mathbf{m}}}(n), \tag{38}$$

from which $\mathbf{Q}_{\mathbf{u}_{\mathbf{m}}}(n)$ can be determined to be

$$\mathbf{Q}_{\mathbf{u}_{\mathbf{m}}}(n) = \mathbf{R}_{\mathbf{m}}(n+1) - \mathbf{R}_{\mathbf{m}}(n). \tag{39}$$

At each step of the Kalman Filter it can be observed (see Appendix A) that the a priori estimates $\hat{\mathbf{m}}^{-}(n+1)$ and $\hat{\mathbf{m}}^{-}(n)$ of $\mathbf{m}(n+1)$ and $\mathbf{m}(n)$, respectively, are available prior to using $\mathbf{Q}_{\mathbf{u}_{\mathbf{m}}}(n)$ in the algorithm. Assuming that, at each time step, the components of the vector $\mathbf{u}_{\mathbf{m}}(n)$ are uncorrelated (i.e. $E\{u_{m_i}(n)\, u_{m_j}(n)\} = 0,\ i \neq j$), a diagonal approximation to the covariance $\mathbf{Q}_{\mathbf{u}_{\mathbf{m}}}(n)$ is proposed, with each diagonal entry being of the form $\breve{Q}\sigma_v^2(n)_{jj}(n) = \hat{m}_j^{-}(n+1)^2 - \hat{m}_j^{-}(n)^2,\ j = 1, \ldots, L_{\mathbf{m}}$, if it is positive, and zero otherwise, which guarantees positive semidefiniteness of the covariance matrix. Finally, a smoothing step is considered that leads to the final estimate $\hat{Q}_{jj}(n)$ of $(\mathbf{Q}_{\mathbf{u}_{\mathbf{m}}})_{jj}(n)$ by defining

$$\hat{Q}_{jj}(n) = \nu_j(n)\, \breve{Q}_{jj}(n) + (1 - \nu_j(n))\ \hat{Q}_{jj}(n-1), \tag{40}$$

where $\hat{Q}_{jj}(n-1)$ is the estimate obtained at the previous iteration and the factor $\nu_j(n)$ is defined as inversely proportional to the square of the difference $\hat{\mathbf{m}}_j^{-}(n+1) - \hat{\mathbf{m}}_j^{-}(n)$.

The variance $\sigma_v^2(n)$ is approximated by $\gamma_0^{-}(n)^2$, where $\gamma_0^{-}(n)$ is the first component of the innovation process defined as the difference between the observed output and the a priori estimated output: $\gamma_0^{-}(n) = y_{\mathrm{QT}}(n) - \hat{y}_{\mathrm{QT}}^{-}(n)$, with $\hat{y}_{\mathrm{QT}}^{-}(n) = \mathbf{s}^T(n)\, \hat{\mathbf{m}}^{-}(n)$.

2.2.1.6. Constrained solution. Estimates of the state vector $\mathbf{m}(n)$ obtained after the application of the Kalman Filter might not satisfy certain constraints that are desirable if physiological inferences are to be derived subsequently. One of the constraints to be placed on the state variables is that they are such that they provide non-negative weights for the linear filter, so that the dependence of QT on each preceding RR interval can be quantified as a proportion (%). The second constraint on the state variables is that the structure of the vector $\mathbf{m}(n)$ (see above) is maintained at all time steps, so that the linear and nonlinear responses can be correctly identified using only the estimate of $\mathbf{m}(n)$ and the consideration of a normalized filter impulse response ($\mathbf{h}^T(n)\ \mathbf{1} = 1,\ \forall n$).

One method for incorporating those constraints into the Kalman Filter is presented next. Such a method is based on one of the approaches described in [15] and used by others (e.g., [16]). According to the constraints described above and noting that $\mathbf{m}_1(n) = a_1(n)\ \mathbf{h}(n)$, a requirement for the constrained estimate (denoted by $\hat{\hat{\mathbf{m}}}(n)$) is that all of the elements in $\hat{\hat{\mathbf{m}}}_1(n)$ are of the same sign (i.e., the absolute value of their sum equals the sum of their absolute values) and, in the case that the order of the nonlinearity is $P = 2$, also that

$$\frac{\hat{\hat{m}}_2(i_1, i_2;\, n)}{\hat{\hat{m}}_1(i_1;\, n)\hat{\hat{m}}_1(i_2;\, n)} = \frac{2}{\prod_{q=0}^{N-1} l_q(i_1, i_2)!}\, \frac{\hat{\hat{m}}_2(0, 0;\, n)}{\hat{\hat{m}}_1(0;\, n)\hat{\hat{m}}_1(0;\, n)}, \tag{41}$$

which is readily derived contrasting the expressions of the first and second-order blocks in $\mathbf{m}(n)$ according to definition (9). For $P = 3$, additional analogous conditions are included regarding expressions involving $\hat{\hat{m}}_3(i_1, i_2, i_3;\, n)$, and so forth for higher order nonlinearities.

To determine the constrained estimates, the constraint surface $\Omega_{\mathbf{m}}$ is built and the constrained Kalman Filter solution is found by projecting the unconstrained state estimate $\hat{\mathbf{m}}(n)$ onto $\Omega_{\mathbf{m}}$. The problem that is solved is as follows:

$$\hat{\hat{\mathbf{m}}}(n) = \arg \min_{\breve{\mathbf{m}}(n) \in \Omega_{\mathbf{m}}} \{(\breve{\mathbf{m}}(n) - \hat{\mathbf{m}}(n))^T\, \mathbf{W}\, (\breve{\mathbf{m}}(n) - \hat{\mathbf{m}}(n))\}, \tag{42}$$

where $\mathbf{W}$ is any $L_{\mathbf{m}} \times L_{\mathbf{m}}$ symmetric positive definite weighting matrix. In the case where $\mathbf{W}$ is chosen as the inverse of the covariance matrix of the a posteriori estimation error

$$\mathbf{W} = \mathbf{P}^{-1}(n), \tag{43}$$

where $\mathbf{P}(n)$ is the estimate of $E\{(\mathbf{m}(n) - \hat{\mathbf{m}}(n))(\mathbf{m}(n) - \hat{\mathbf{m}}(n))^{\mathrm{T}}\}$ obtained at the iteration n of the Kalman Filter, it is readily seen that $\hat{\hat{\mathbf{m}}}(n)$ is a maximizer of the gaussian probability density $N(\hat{\mathbf{m}}(n), \mathbf{P}(n))$ satisfying the required constraints [16]. The obtained estimate $\hat{\hat{\mathbf{m}}}(n)$ is taken as the final representation of the state of the global system at time n and is used in subsequent iterations of the adaptive filter for the estimation of future states. For the sake of simplicity, in the following we denote the constrained estimate by $\hat{\mathbf{m}}(n)$ in substitution of $\hat{\hat{\mathbf{m}}}(n)$.

2.2.2. Nonlinearized-Unscented Kalman Filter approach (N-UKF)

The second way to solve the system identification problem uses adaptive recursive nonlinear filters to estimate the state of the system at each time instant. In that case, the measurement equation is not transformed into a linear combination of functions of the input signal and, accordingly, a nonlinear state-space problem is defined. To solve it, the Unscented Kalman Filter (UKF) [17,18] is used. This is described below.

2.2.2.1. State-space formulation. The output $y_{\mathrm{QT}}(n)$ of the global system is now expressed as

$$y_{\mathrm{QT}}(n) = f(\mathbf{x}_{\mathrm{RR}}(n),\, \mathbf{c}(n)) + v(n), \tag{44}$$

where $\mathbf{c}(n)$ is the vector of length $L_c = P + N + 1$ given by

$$\mathbf{c}(n) = [\mathbf{a}^{\mathrm{T}}(n)\, \mathbf{h}^{\mathrm{T}}(n)]^{\mathrm{T}} \tag{45}$$

and

$$f(\mathbf{x}_{\mathrm{RR}}(n),\, \mathbf{c}(n)) = \sum_{k=0}^{P} c_k(n) \left(\sum_{i=P+1}^{P+N} c_i(n) x_{\mathrm{RR}}(n - i + P + 1) \right)^k. \tag{46}$$

The expression above (44) for $y_{QT}(n)$ constitutes the *measurement equation* of the state-space formulation of our problem. For the *process equation*, information about the nature of the temporal evolution of the system state is unavailable; therefore, a random-walk model of the form

$$\mathbf{c}(n+1) = \mathbf{c}(n) + \mathbf{u}_{\mathbf{c}}(n), \quad n \geq 0 \tag{47}$$

is considered, where $\mathbf{u_c}(n)$ is a zero-mean white noise process with covariance matrix $\mathbf{Q}_{\mathbf{u_c}}(n)$ and uncorre-lated with $v(n)$. In addition, the initial state $\mathbf{c}(0)$ is assumed to be a random vector that has mean $\boldsymbol{\mu}_{0,\mathbf{c}}$ and covariance $\Pi_{0,\mathbf{c}}$ and is uncorrelated with $v(n)$ and $\mathbf{u_c}(n)$. In our implementation of the recursive nonlinear filtering algorithm, $\boldsymbol{\mu}_{0,\mathbf{c}}$ is defined by joining the vectors $\boldsymbol{\mu}_{0,\mathbf{a}}$ and $\boldsymbol{\mu}_{0,\mathbf{h}}$ described in Section 2.2.1 and the matrix $\Pi_{0,\mathbf{c}}$ is taken as the identity matrix. In our estimation problem, the matrices $\mathbf{Q}_{\mathbf{u_c}}(n)$ and $\sigma_v^2(n)$ are not known and need to be estimated.

2.2.2.2. Regularization. The regularization procedure is analogous to the one described in Section 2.2.1, but now the nonlinear measurement equation is augmented considering the following definitions: $\varphi(n) = \mathbf{0}$, $\mathbf{R}_{\mathbf{v}'}(n) = \mathbf{I}$ and $\Phi(n)$ the $(N-1) \times L_{\mathbf{c}}$ linear operator with associate matrix having 0-value in the first $P+1$ columns (those corresponding to the nonlinearity coefficients) and containing the matrix $\mathbf{D^1}(n)$ defined in Section 2.2.1 in the last N columns (corresponding to the filter weights):

$$\Phi(n) = \beta(n)[\mathbf{0} \;\; \mathbf{D}^{\mathbf{1}}(n)]. \tag{48}$$

The new measurement equation is expressed as

$$\tilde{\mathbf{y}}_{QT}(n) = \tilde{f}(\mathbf{x}_{RR}(n), \mathbf{c}(n)) + \tilde{\mathbf{v}}(n), \tag{49}$$

where

$$\tilde{f}(\mathbf{x}_{RR}(n), \mathbf{c}(n)) = \begin{bmatrix} f(\mathbf{x}_{RR}(n), \mathbf{c}(n)) \\ \Phi(n)\,\mathbf{c}(n) \end{bmatrix}. \tag{50}$$

2.2.2.3. Unscented Kalman Filter. The nonlinear procedure used to solve the state-space problem (see (47) and (49)) is based on the Unscented Kalman Filter (see Appendix B). Unlike the more commonly used Extended Kalman Filter (EKF), which replaces nonlinear functionals with their first order Taylor approximations, the UKF maintains the exact nonlinearities and approximates the posterior distributions by gaussians [17]. Those approximations are performed by generating a set of deterministically chosen points called *sigma points*, which capture the true mean and covariance of the random state vector. When the sigma points are propagated through the nonlinear function, they produce a new set of points that can be used to estimate the mean and covariance of the nonlinearly transformed vector.

Based on that concept, the UKF can be described as a recursive minimum mean-square error (MMSE) estimator that performs three basic operations during each of its iterations; namely, computation of sigma points, time-update (i.e., projection in time of the actual estimates to get a priori estimates for the next step), and measurement-update (i.e., correction of the a priori estimates by using the observed output).

In our study, where the process equation is assumed to be linear and the measurement equation is described by the nonlinear function $\tilde{f}$, the Unscented Kalman Filter is accurate to the third order in the case where the prior state distribution and the process and measurement errors are gaussian, or at least to the second order if they are non-gaussian [17]. Consequently, the UKF achieves higher accuracy than the first-order EKF. That improvement is not at the expense of more computational demand, which is of the same order than that of the EKF, and furthermore, the UKF is more widely applicable than the EKF because it does not require the computation of derivatives with respect to the state variables and, consequently, it can be applied for non-differentiable functions.

In this study, the UKF is used to solve the nonlinear state-space problem previously formulated and an estimate $\hat{\mathbf{c}}(n)$ of the time-varying state vector $\mathbf{c}$(n) is obtained.

2.2.2.4. Estimation of noise covariances. On-line estimation of the matrix $\mathbf{Q}_{\mathbf{u_c}}(n)$ and the scalar $\sigma_v^2(n)$ is performed following the same method used in the VL–KF approach and, in this case, it is integrated into the UKF algorithm.

2.2.2.5. Constrained solution. The constrained UKF estimates are derived in a manner analogous to the one used in the VL–KF approach, with the only difference found in the definition of the constraint surface $\Omega_{\mathbf{c}}$. The constrained solution $\hat{\tilde{\mathbf{c}}}(n)$ is forced to comply with: $\hat{\tilde{c}}_{P+1}(n) \geq 0, \ldots, \hat{\tilde{c}}_{P+N}(n) \geq 0$ and $\hat{\tilde{c}}_{P+1}(n) + \ldots + \hat{\tilde{c}}_{P+N}(n) = 1$:

$$\hat{\tilde{\mathbf{c}}}(n) = \arg \min_{\breve{\mathbf{c}}(n) \in \Omega_{\mathbf{c}}} \{(\breve{\mathbf{c}}(n) - \hat{\mathbf{c}}(n))^T \mathbf{W}(\breve{\mathbf{c}}(n) - \hat{\mathbf{c}}(n))\}, \tag{51}$$

where $\mathbf{W}$ is any $L_{\mathbf{c}} \times L_{\mathbf{c}}$ symmetric positive definite weighting matrix. The solution to the problem provides the desired constrained state estimate $\hat{\tilde{\mathbf{c}}}(n)$, which will be used in forthcoming iterations of the adaptive filter. To simplify the notation, $\hat{\tilde{\mathbf{c}}}(n)$ is replaced with $\hat{\mathbf{c}}(n)$.

3. Data

3.1. Simulated data

To assess the performance of the two adaptive procedures proposed in this study, simulations were performed under different scenarios. In all of the simulation cases, a real RR series from the population that will be described in Section 3.2 was considered as input signal. To perform the simulations, repetition of three times the RR series was performed to be able to set the length of the input signal at $N_T = 15{,}000$ samples.

The values of the system parameters $\mathbf{h}(n)$ and $\mathbf{a}(n)$ were established and the corresponding output signals were generated, including the addition of white gaussian noise (w.g.n.) with an SNR of 20 dB. Those input and output signals constitute all of the information provided to the algorithm, which tries to estimate the actual parameter values.

In the first type of simulation (type I), the system parameters $\mathbf{h}(n)$ and $\mathbf{a}(n)$ are considered to be time-invariant:

- for the first simulation test I.1, a linear filter with impulse response $\mathbf{h}(n) = [0.5714\ 0.2857\ 0.1429]^{\mathrm{T}}$ and a first-order Taylor polynomial with coefficients $\mathbf{a}(n) = [0.3\ 0.12]^{\mathrm{T}}$ are considered,
- a second simulation test I.2 is performed using the same time-invariant impulse response as in I.1 and time-invariant coefficient vector $\mathbf{a}(n)$ containing the coefficients of a quadratic nonlinear function: $\mathbf{a}(n) = [0.3\ 0.12\ -0.08]^{\mathrm{T}}$.

The same type of simulation using nonlinear functionals of order higher than two was not pursued in this study because first and second-order nonlinearities are sufficient for application to the analysis of repolarization adaptation.

In the second type of simulation (type II), the linear filter $\mathbf{h}(n)$ is considered to be time-variant, while the nonlinearity coefficients remain time-invariant:

- for simulation test II.1, vector $\mathbf{a}(n)$ is taken as $\mathbf{a}(n) = [0.3\ 0.12]^{T}$, while vector $\mathbf{h}(n)$ is defined as a normalized decreasing exponential of factor $\alpha(n)$, with $\alpha(n)$ generated from a Markov model of the form $\alpha(n+1) = \alpha(n) + u_{\alpha}(n)$, where $u_{\alpha}(n)$ is zero-mean w.g.n. with variance $\sigma_{\alpha}^2(n)$, $\sigma_{\alpha}(n) = 10^{-3}$, and the initial value is taken to be $\alpha(0) = 0.5$,
- simulation test II.2 is elaborated on the same basis as test II.1, except that a second-order Taylor polynomial, $\mathbf{a}(n) = [0.3\ 0.12\ -0.08]^{\mathrm{T}}$, is used.

The third type of simulation (type III) deals with the more general case in which both the linear and nonlinear portions of the global system are time-variant. The components of the vectors $\mathbf{a}(n)$ and $\mathbf{h}(n)$ are built up from Markov models considering

- a time-varying first-order nonlinearity in test III.1,
- a time-varying second-order nonlinearity in test III.2.

In this third type, the covariance matrix of zero-mean w.g.n. $\mathbf{u}_{\mathbf{a}}(n)$ in equation $\mathbf{a}(n+1) = \mathbf{a}(n) + \mathbf{u}_{\mathbf{a}}(n)$ is defined as $\sigma_{\mathbf{a}}^2(n)\mathbf{I}$, with $\sigma_{\mathbf{a}} = 10^{-3}$, and the initial vector $\mathbf{a}(0)$ is defined as in tests II.1 and II.2, respectively.

3.2. Real data

This study evaluated ECG recordings obtained from 33 healthy subjects during controlled postural manoeuvring. Continuous 12-lead electrocardiograms, sampled at 500 Hz, were recorded while subjects were changing their posture from supine to sitting, from sitting to standing, ..., which resulted in substantial and, frequently, very abrupt changes in heart rate. Those types of recordings provided us with a very useful resource for analyzing the mode of adaptation of the QT interval and the T_{a} index to accelerations and decelerations in heart rate. The durations of the recordings varied from 50 min to 2 h.

For each ECG recording, the lead that had the greatest signal-to-noise ratio was identified. On that lead, RR and QT intervals, as well as T wave amplitudes, were measured using the automatic wavelet transform-based delineation system described in [19], which was previously validated using annotated standard databases. To remove potential outliers from the obtained RR, QT, and T_{a} series, a procedure that uses a Median Absolute Deviation (MAD) filter [20] was applied. Subsequently, the clean series were interpolated linearly at a sampling frequency of 1 Hz and low-pass filtered with a cutoff frequency of 0.05 Hz to avoid the sympathetic and parasympathetic variability influences of the Autonomic Nervous System.

4. Performance measures

4.1. Parameter estimation evaluation

The performance of the two proposed algorithms described in Section 2.2 is evaluated for the problem of estimating $\mathbf{h}(n)$ and $\mathbf{a}(n)$. For that purpose, a number $N_{\mathrm{rea}} = 50$ of Monte Carlo runs are considered for each simulation test. In each run, different realizations of the noise $v(n)$ and of the system vectors $\mathbf{h}(n)$ and $\mathbf{a}(n)$ are generated (except for those tests where $\mathbf{h}(n)$ and $\mathbf{a}(n)$ are deterministic). Let $\hat{\mathbf{h}}^{(j)}(n)$ denote the estimate of the actual vector $\mathbf{h}^{(j)}(n)$ at the j-th Monte Carlo run, $j = 1, \ldots, N_{\mathrm{rea}}$. Analogously, let $\hat{\mathbf{a}}^{(j)}(n)$ denote the estimate of $\mathbf{a}^{(j)}(n)$. The estimation errors are denoted by $\varepsilon_{\mathbf{h}}^{(j)}(n) = \mathbf{h}^{(j)}(n) - \hat{\mathbf{h}}^{(j)}(n)$ and $\varepsilon_{\mathbf{a}}^{(j)}(n) = \mathbf{a}^{(j)}(n) - \hat{\mathbf{a}}^{(j)}(n)$.

A measure of the algorithmic performance is given by the root mean square (RMS) of the estimation errors, both in the estimation of the filter weights and the nonlinearity coefficients:

$$r\{\widehat{\varepsilon_{h_i}(n)}\} = \left(\frac{1}{N_{\mathrm{rea}}}\sum_{j=1}^{N_{\mathrm{rea}}}\left(\varepsilon_{h_i}^{(j)}(n)\right)^2\right)^{1/2}, \quad i = 0, \ldots, N-1, \tag{52}$$

$$r\{\widehat{\varepsilon_{a_k}(n)}\} = \left(\frac{1}{N_{\mathrm{rea}}}\sum_{j=1}^{N_{\mathrm{rea}}}\left(\varepsilon_{a_k}^{(j)}(n)\right)^2\right)^{1/2}, \quad k = 0, \ldots, P. \tag{53}$$

4.2. Adaptation markers

To provide insights into the QT/RR and T_{a}/RR relationships, the approaches developed in Section 2 were applied to the real data. Before processing, repetition of three times the RR, QT, and T_{a} series was performed and results corresponding to the last repetition were kept for subsequent analysis. In each recording, a measurement of the error in the estimation of the signal at the output of the system is given by the RMS of the prediction error, which is the difference between the actual output signal $y_{\mathrm{QT}}(n)$ and the estimated output signal $\hat{y}_{\mathrm{QT}}(n)$ (respectively, $y_{T_{\mathrm{a}}}(n)$ and $\hat{y}_{T_{\mathrm{a}}}(n)$), calculated individually for the two proposed methodologies and orders $P = 1$ and 2:

$$\varepsilon = \left(\frac{1}{N_I}\sum_{n=0}^{N_{I-1}}\left(y_{\mathrm{QT}}(n) - \hat{y}_{\mathrm{QT}}(n)\right)^2\right)^{1/2}, \tag{54}$$

where N_I is the length of the series $y_{QT}(n)$, which varies from record to record, and $\hat{y}_{QT}(n) = g(\hat{\mathbf{h}}^T(n)\,\mathbf{x}_{RR}(n),\ \hat{\mathbf{a}}(n))$.

Using the ultimate system state estimates, associated with the selected order and methodology, a quantitative measurement of the time that each of the analyzed repolarization indices (QT and T_a) needs to adapt to a change in heart rate is defined by the variable $L_{90}(n)$, which is calculated for each adaptation profile $\hat{\mathbf{h}}(n)$ using the exponential model that approximates it. That quantity generalizes the measurement L_{90} introduced in [5] and it is defined to cover 90% of the total adaptation, thus accounting for the preceding RR intervals which are notably influential on the corresponding repolarization measurement at time n. The exponential approximation for $\hat{\mathbf{h}}(n)$ is of the form $\hat{h}_i(n) \approx \kappa(n)\alpha^i(n),\ \ i = 0, \ldots, N-1$, and its extension up to a length $\breve{N} = 300$ (the same used in [5]) is considered:

$$\breve{h}_i(n) = \breve{\kappa}(n)\alpha^i(n),\ i = 0, \ldots, \breve{N} - 1, \tag{55}$$

where $\breve{\kappa}(n)$ in (55) is a normalizing constant. Denoting the cumulative sum by $\breve{h}_i(n) = \sum_{j=i}^{\breve{N}-1} \breve{h}_j(n)$, $i = 0, \ldots, \breve{N} - 1$, and applying a threshold $\eta = 0.1$ to it, it can be readily seen that the first index i_0 for which $\breve{h}_{i_0}(n) < \eta$ is:

$$i_0 = [\log_{\alpha(n)}(\eta + \alpha^{\breve{N}}(n)(1-\eta))]. \tag{56}$$

The measurement $L_{90}(n)$ is defined as the time in seconds expressed by i_0. It can be observed that for $0 < \alpha(n) < 1$ and $\breve{N}$ large, the expression above can be approximated by:

$$L_{90}(n) = [\log_{\alpha(n)}\eta] = \left[\frac{\ln \eta}{\ln \alpha(n)}\right], \tag{57}$$

which depends only on the factor $\alpha(n)$ derived in the estimation procedure. With this proposed measurement we are able to quantify, at each instant of the recording, the time required for the examined index (QT or T_a) to follow an RR change.

In each recording, the values of $L_{90}(n)$ were assessed as a function of the rate of change (i.e. numerical gradient) in the RR series, being that rate denoted in the following by $\lambda(n)$. The function defined by the pairs $[\lambda(n), L_{90}(n)]$ was afterward linearly interpolated so as to have the adaptation time $L_{90}(n)$ calculated for specific values of the rate of change in RR. This facilitates the comparison of recordings and allows their averaging.

5. Results

5.1. Simulation results

For the estimation process in the simulation tests, the orders of the filter and the nonlinear function were not known a priori and were set to $N = 5$ and $P = 1$, respectively, for the estimation in test I.1. The two algorithms (VL–KF and N-UKF) correctly identified the order of the actual linear filter, and generated fourth and fifth weight values that were very close to zero. The estimated values of the first three weights in $\hat{\mathbf{h}}(n)$ and of the nonlinearity coefficients in $\hat{\mathbf{a}}(n)$ successfully approximated their theoretical counterparts, which led to the small error measurements $r\{\varepsilon_{\mathbf{h}}(n)\}$ and $r\{\varepsilon_{\mathbf{a}}(n)\}$ presented in Fig. 2, using dotted green line for VL–KF and dotted magenta line for N-UKF. As it can be seen from Fig. 2, $r\{\varepsilon_{\mathbf{h}}(n)\}$ takes values that are, in mean along time, always below 0.026 n.u. for any of the two methodologies. The values of $r\{\varepsilon_{\mathbf{a}}(n)\}$ are in mean below 0.001 n.u. The estimation process for test I.2 was performed

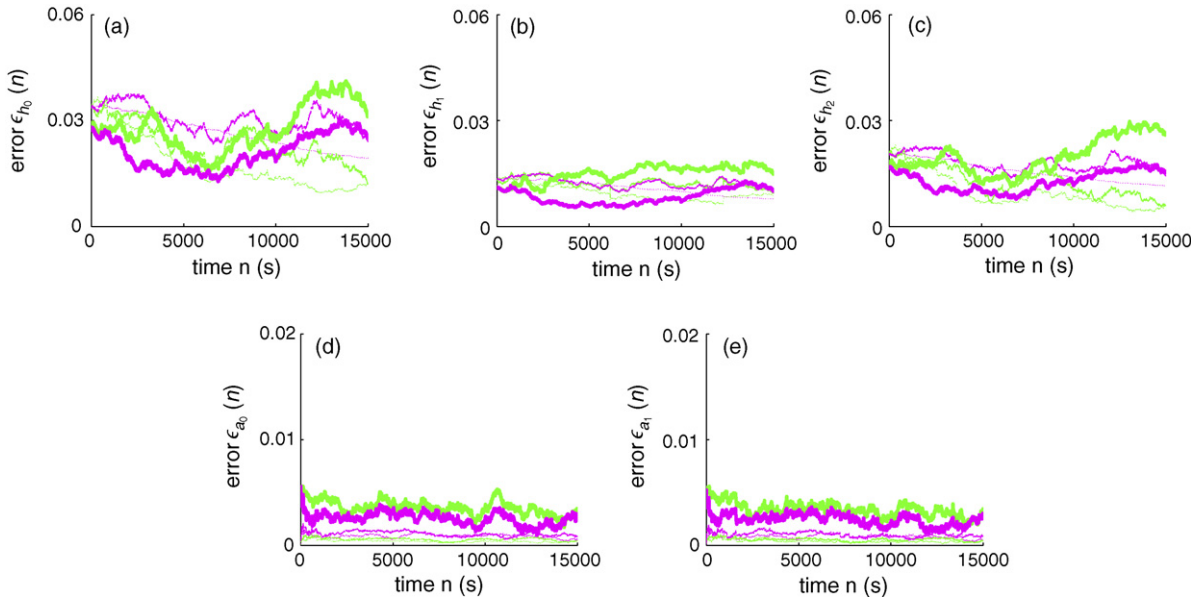

Fig. 2. In (a), (b) and (c), root mean square of the estimation errors $\varepsilon_{h_0}(n)$, $\varepsilon_{h_1}(n)$, and $\varepsilon_{h_2}(n)$, respectively, are presented for tests I.1 (dotted line), II.1 (dashed line) and III.1 (solid line). Panels (d) and (e) show results corresponding to $\varepsilon_{a_0}(n)$, and $\varepsilon_{a_1}(n)$, respectively. In each graphic, green line is associated to the VL–KF methodology, while magenta line corresponds to N-UKF. (For interpretation of the references to color in this figure legend, the reader is referred to the web version of the article.)

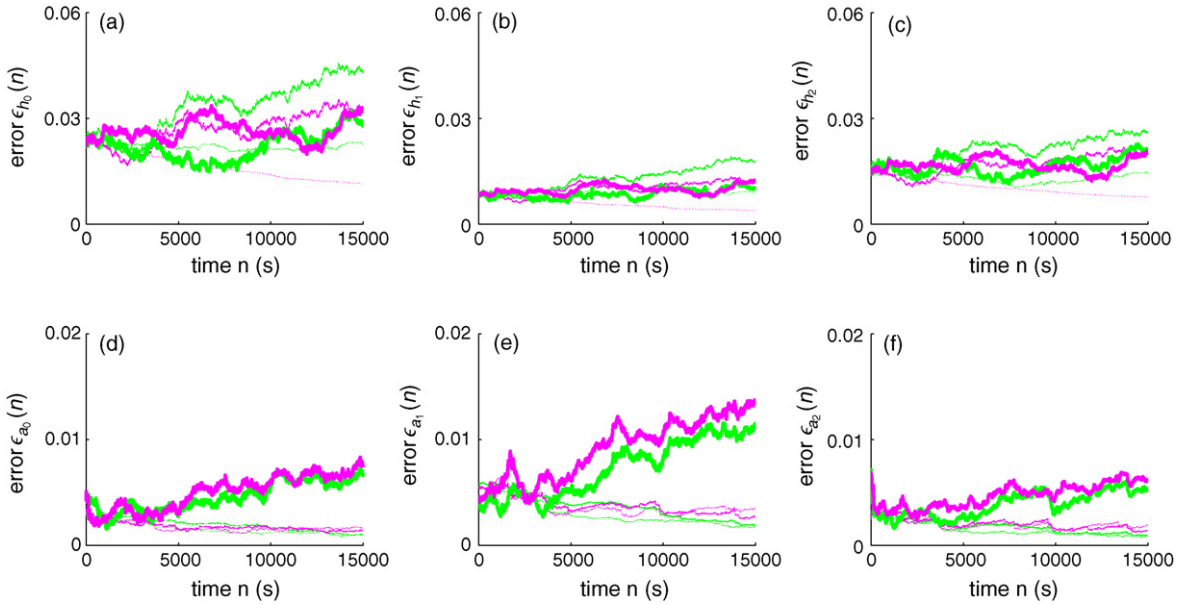

Fig. 3. In (a), (b) and (c), root mean square of the estimation errors $\varepsilon_{h_0}(n)$, $\varepsilon_{h_1}(n)$, and $\varepsilon_{h_2}(n)$, respectively, are presented for tests I.2 (dotted line), II.2 (dashed line) and III.2 (solid line). Panels (d), (e) and (f) show results corresponding to $\varepsilon_{a_0}(n)$, $\varepsilon_{a_1}(n)$, and $\varepsilon_{a_2}(n)$, respectively. In each graphic, green line is associated to the VL–KF methodology, while magenta line corresponds to N-UKF. (For interpretation of the references to color in this figure legend, the reader is referred to the web version of the article.)

using the same orders N and P than those used to simulate. That is also applicable to all of the subsequent tests. In test I.2, the high coincidence between the converged estimated values and the actual values is shown in Fig. 3 using the same line format as in test I.1. In this case, the mean values of $r\{\widehat{\varepsilon_{\mathbf{h}}(n)}\}$ and $r\{\widehat{\varepsilon_{\mathbf{a}}(n)}\}$ are always inferior to 0.022 and 0.004 n.u., respectively.

In test II.1, the two proposed estimation procedures were able to track the temporal variations in the simulated weights and led to a quick convergence in the approximation of the nonlinearity coefficients, which is illustrated in Fig. 2 using dashed green line for the VL–KF methodology and dashed magenta line for N-UKF. The results from test II.2 are shown in Fig. 3. The mean of the errors $r\{\widehat{\varepsilon_{\mathbf{h}}(n)}\}$ and $r\{\widehat{\varepsilon_{\mathbf{a}}(n)}\}$ in test II.1 is below 0.031 and 0.001 n.u., respectively, for any of the two tested methodologies. For test II.2, they are below 0.033 and 0.004 n.u.

The outcomes from the third type of simulation are depicted in Fig. 2 for test III.1 and in Fig. 3 for test III.2. In this case errors are larger than in the other two previous types of simulation, with the mean of $r\{\widehat{\varepsilon_{\mathbf{h}}(n)}\}$ and $r\{\widehat{\varepsilon_{\mathbf{a}}(n)}\}$ upper bounded by 0.028 and 0.004 n.u., respectively, in test III.1, and by 0.027 and 0.009 n.u. in test III.2.

The simulation analysis demonstrated that the two approaches (VL–KF and N-UKF) had minimal differences in the estimation and they produced very good agreement between simulated and estimated quantities. For cases where the order of the Taylor polynomial is $P = 1$, any choice is appropriate and the VL–KF methodology is suggested for performing the estimation. When the order P of the nonlinearity is two or higher and the order N of the linear filter is large, the number of parameters to be estimated using the VL–KF procedure increases substantially and, in those cases, the N-UKF is suggested as more convenient.

5.2. ECG analysis

When the procedures developed in our study are used to investigate the mode of adaptation of QT and T_a to changes in heart rate on a beat-to-beat basis, the effect of the nonlinearity order ($P = 1$ or 2) is, first of all, analyzed. According to the simulation results presented in Section 5.1, the methodology used for the case $P = 1$ is VL–KF, while N-UKF is used when $P = 2$. In each recording, the root mean square error given in (54) is evaluated for both orders. In the case of the QT interval, the two order cases ($P = 1$ and 2) had minor differences that were always below 1 ms (around 1.5% of the total QT variation) for all of the analyzed recordings and all of the tested filter lengths ($N = 1$, 3, 5, 10, 15, 20, 50). Furthermore, the interpretation of the findings in terms of weight distributions is totally equivalent in both order cases. Consequently, it can be concluded that the relationship between QT and $\overline{\text{RR}}$ is adequately modeled by a time-varying first-order Taylor polynomial and, therefore, the interpretation of the nonlinearity evolution is accomplished in terms of the intercept and the slope, only. In that case, the VL–KF approach is justified because $P = 1$ is used. However, when the analogous study is performed for the T_a index, greater differences in the prediction error are found between the cases $P = 1$ and 2. In particular, for over one third of the recordings, differences of more than 30 μV (around 10% of the total T_a variation) could be found in favour of $P = 2$ versus $P = 1$. This implies that, for modeling the relationship between T_a and RR, a second-order nonlinearity is more suitable than a first-order one. Consequently, the N-UKF approach is used, since the order $P = 2$ has been selected.

Once the nonlinearity order was set to $P = 1$ for QT and $P = 2$ for T_a, the order N of the linear portion had to be

identified. As expected, when N was increased, the RMS of the prediction error, ε, was diminished. On the other hand, it was demonstrated in [5] that, from a clinical perspective, the initial 50 preceding RR intervals are the most relevant in the analysis of QT/RR adaptation. Therefore, in this study, the value $N = 50$ was established and it was corroborated that the error ε associated with that value was below 25% of the preliminary error calculated with $N = 1$ (when the RR memory effect is not taken into account) in more than 80% of the recordings, for the analysis of the QT interval. In the case of the T_a index, the error decreased to 60% of its initial value (with $N = 1$) for the last tested N value ($N = 50$), with the observation that, in this case, low values of N (up to N = 15) already contribute to substantial error decrease.

An example of how the proposed procedure can be used to assess dynamically the relationship between the QT and RR intervals is presented next. Fig. 4(a) and (b) contain the RR and QT interval series corresponding to one of the recordings analyzed in the study. The beat-to-beat evolution of the linear filter weights is shown in Fig. 4(c) and (d) for a linear filter of length $N = 50$. Panel 4(c) shows the summed contribution of the first 10 weights (i.e., those associated with the most recent RR intervals, which are expected to most strongly influence each QT measurement), and panel 4(d) shows the contribution of the remaining weights up to the order of the linear filter. The relative contribution of the first RR intervals compared to that of more distant RR intervals can be evaluated along the recording and differences in the QT adaptation for segments of steady and non-steady heart rate can be assessed. It can be observed that distant RR intervals are more influential during periods of change in HR. The progression of the nonlinearity coefficients calculated from the same recording is shown in Fig. 4(e) and (f). Variations in $\hat{a}_1(n)$ reflect how the QT/$\overline{\text{RR}}$ relationship becomes more/less steep after decelerations/accelerations in heart rate. Analogously, the relationship between T_a and RR was investigated. In this case a delay effect in the adaptation to HR changes could also be observed, even though less marked than for QT. However, no significant differences in the adaptation of T_a to marked HR changes as compared to stable periods could be found. As for the nonlinearity coefficients, their visualization reveals that $\hat{a}_1(n)$ and $\hat{a}_2(n)$ are as well noticeably altered after rate changes.

It is of particular interest to analyze the QT/RR relationship in the presence of a very abrupt change in HR. We selected an excerpt from the recording of Fig. 4 that presents this characteristic. The corresponding excerpts of RR and QT

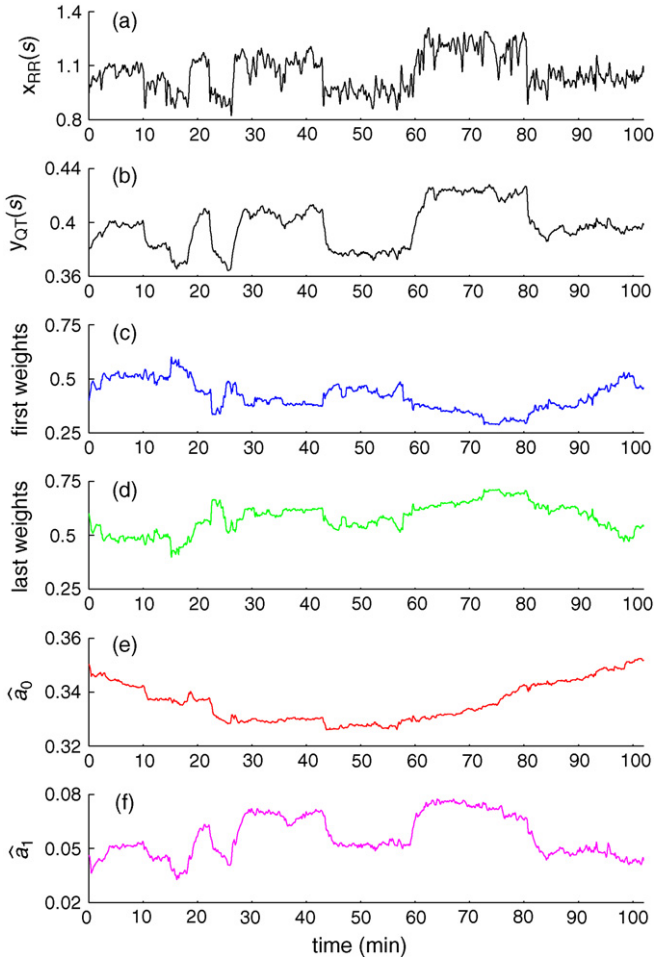

Fig. 4. In (a) and (b), the RR and QT interval series for one of the recordings analyzed in the study are plotted. In (c) and (d), the temporal evolution of the linear filter weights identified for the series presented in (a) and (b) is illustrated. Specifically, panel (c) shows the contribution of the first 10 weights of the linear subsystem, and panel (d) contains the contribution of the remaining weights up to the order of the linear FIR filter, which was set to 50 in this study. In (e) and (f), the temporal evolution of the nonlinearity coefficients identified for the series in (a) and (b) is presented.

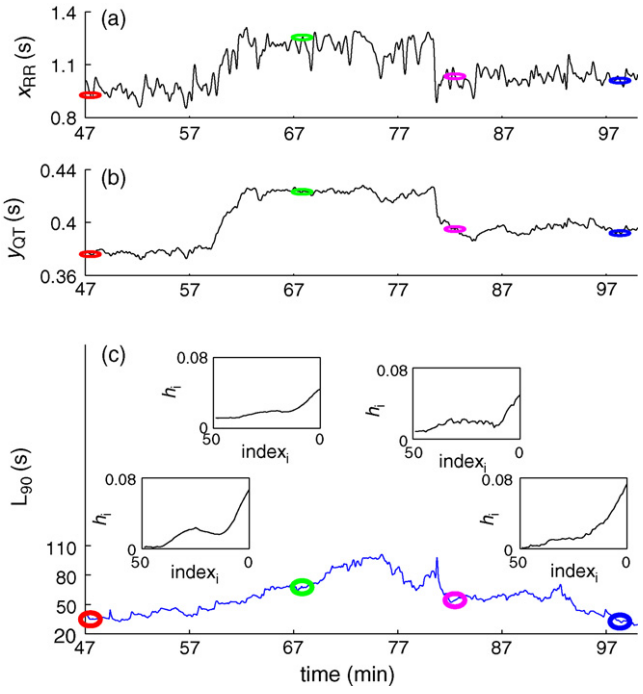

Fig. 5. A segment of Fig. 4 illustrating a marked change in heart rate was selected and the corresponding RR and QT interval series are plotted in (a) and (b). Circles indicate points selected for subsequent analysis. Panel (c) shows the time for QT adaptation measured by the variable L_{90} (defined in Section 4.2) for the selected segment, together with the optimum QT/RR adaptation profiles extracted at time instants indicated with circles in panel (c).

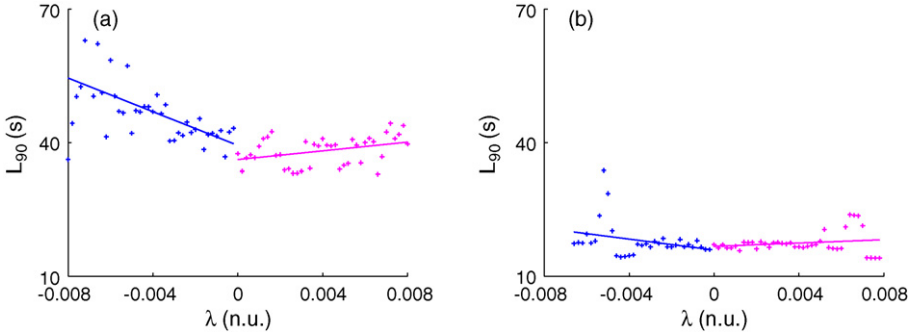

Fig. 6. In (a), the adaptation time L_{90} required by QT to follow RR is presented as a function of the rate of change λ in the RR series. The pairs [λ, L_{90}], shown as '+', are obtained after interpolation and subsequent averaging over recordings (see text for details). Lines fitting those pairs, both for heart rate accelerations and decelerations, are presented as well. In (b) analogous results are shown for the T_a index.

interval series are plotted in Fig. 5(a) and (b), and segments of stable, decelerating, and accelerating heart rate are evident. From that excerpt, a plot of the QT adaptation time measured at each time instant by the marker $L_{90}(n)$ described in Section 4.2 is presented in Fig. 5(c). The QT lag after the decelerating rate change is around 1.5 min for that particular recording. The adaptation profiles $\hat{\mathbf{h}}(n)$ of representative instants of the excerpt are plotted in the same figure. Those adaptation profiles $\hat{\mathbf{h}}(n)$ permit the visualization of the dependence of QT on RR intervals previous to the immediately preceding interval. Each adaptation profile is plotted as a function of the weight index i, where i is varied from $N-1$ to 0 for ease of interpretation.

The qualitative results presented for a given subject of the database can be quantified for all of the recordings by representing the interpolated $L_{90}(n)$ calculated at specific values of $\lambda(n)$. Graphics obtained for individual recordings were very similar in shape and scale, and, consequently, the average of all of them is considered as representative. The mean pairs $[\lambda(n), L_{90}(n)]$ are shown as '+' in Fig. 6(a) (for the QT interval) and Fig. 6(b) (for T_a). A line fitting those pairs is represented as well to facilitate interpretation of the results. From Fig. 6(a) it can be concluded that the larger the changes in RR, the longer is the time required by the QT interval to follow those changes. Specifically, for RR variations of magnitude $\lambda(n) = 0.008$ n.u., it takes QT nearly 1 min to complete its adaptation. The observation that $L_{90}(n)$ increases as a function of the absolute rate of change in RR (i.e. $|\lambda(n)|$) is valid both for heart rate accelerations and heart rate decelerations. Regarding the T_a index, the results point out in the same direction as for the QT interval. However, the effect is less manifested than for QT, being in this case the adaptation times at extreme RR variations always below 30 s.

6. Discussion

In this study two procedures were proposed for identification of a time-varying nonlinear system with memory operating under nonstationary conditions, which models the time-varying relationship between a repolarization index (QT or T_a) and the RR interval. To determine which of the procedures, described in Sections 2.2.1 and 2.2.2, is most appropriate for solving the identification problem, simulations were run in a realistic scenario and algorithmic performances were evaluated using the criterion of minimum root mean square of the estimation errors. For the simulations, orders $P = 1$ and 2 of the nonlinear subsystem were tested because they are sufficient plausible values for modeling the QT/RR and T_a/RR relationships within a small vicinity of a given RR value [5,22]. In all of the simulations, the length N of the linear filter was considered to be three because this allowed the representation of all of the estimated quantities and the visual assessment of the tracking performance of the algorithms. When simulations were run for larger values of N, slightly greater error values occurred, but the same conclusions on the algorithmic performance could be drawn. Based on our chosen figure of merit (i.e., the root mean square), when the order P of the polynomial is one, the method that uses linearization through Volterra expansion and subsequent estimation using the Kalman Filter (VL–KF) provided estimates that were practically equal to those rendered by the method that deals directly with the nonlinear estimation using the Unscented Kalman Filter (N-UKF). For situations in which the order of the polynomial is two (or higher), and the number of weights of the linear filter is great, the linearized procedure is not feasible because the total number of parameters to be estimated increases very substantially and, accordingly, the nonlinearized procedure N-UKF is recommended. According to our simulation results, the N-UKF provides as accurate estimates as VL–KF in that case.

When the proposed procedures were used to analyze the QT interval adaptation in response to changes in HR and nonlinearity orders $P = 1$ and 2 were compared, the differences were insignificant, which indicates that practically no improvement is achieved when quadratic nonlinearities are considered. In light of that, the VL–KF approach with a value for P equal to 1 is selected. Although the results obtained for $P = 1$ and 2 are very similar, that does not imply that the $[\mathrm{QT}, \overline{\mathrm{RR}}]$ data of the entire recording are fitted adequately by a linear regression model because, in this study, the nonlinearity $g(\cdot)$ is considered to be time-varying and, consequently, it models the $[\mathrm{QT}(n), \overline{\mathrm{RR}}(n)]$ data pairs in a neighbourhood of each averaged RR measurement. Moreover, even considering the nonlinearity behaviour in a small neighbourhood of each point, only, it is not a priori assumed that $P = 1$ is appropriate

but it is concluded from the results. On the other hand, investigation of T_a adaptation to heart rate revealed more substantial differences between the orders $P = 1$ and 2, confirming that a first-order Taylor polynomial is insufficient to describe the T_a dependence on RR. The above discussed results as well as all the other results described in the present study were obtained considering that the RR, QT and T_a series were sampled at a frequency of 1 Hz. Even this sampling frequency may seem to be too low, additional studies carried out using higher sampling frequencies revealed minor differences in the outcome of the identification algorithm that, accordingly, led to the same interpretation of the results.

In the analysis of the relationship between the QT and RR intervals, it is reasonable to speculate that the dependence of QT on heart rate can have different characteristics depending on whether the recording segment being analyzed corresponds to a period when HR is stable or, conversely, when there are abrupt variations in HR. The recordings used in this study were obtained from subjects performing a protocol of body postural changes; therefore, at certain time instants the RR signal exhibits marked changes to which the QT reacts, but not instantaneously. When that QT response is investigated using the method that we have proposed, the contribution of the most recent RR intervals, relative to that of more distant RR intervals, tends to decrease after the occurrence of a sudden and marked change in HR. The variable $L_{90}(n)$ that measures the QT adaptation time is able to reflect that effect, as reported in Section 5.2, where it was shown that the larger the magnitude of RR change, the longer is the time needed by the QT interval to adapt to it, with QT lags found after abrupt HR changes being close to 1 min. The results of this study are consistent with the findings in [23] regarding pacing rate and those in [5] for 24-h ambulatory recordings, with the difference that the adaptation times measured on young healthy subjects are substantially smaller than those found on post-MI patients (approximately 2.5 min) [5] or in patients with complete heart block (up to 3 min) [23]. The method proposed here has the advantage of being able to dynamically provide an estimate of the adaptation time along the recording period. In the case of the T_a index, the adaptation lag is somewhat less pronounced, as reflected by the results given in Section 5.2, and it remains more constant along the recording period.

In addition, information can be extracted from the coefficients of the nonlinearity relating QT and $\overline{RR}$ in the proposed model. When there is a sudden deceleration in rate, the slope increases initially, while a sudden acceleration in HR is followed by an instantaneous decrease in the slope values (see Fig. 4(f)). Similar conclusions are extracted for the nonlinear function relating T_a and RR.

7. Conclusions

This study presents and validates a new methodology to dynamically assess adaptation of repolarization to RR changes, accounting for the effect of hysteresis. Over real ECG recordings of healthy subjects, it is demonstrated that the time needed by the QT interval to follow RR changes increases as a function of the RR variation rate. The response of the T wave amplitude (T_a) to RR changes is shown to be substantially faster than that of QT. Also, while the T_a/RR relationship is proved to be locally quadratic, the QT/RR relationship is found to be well approximated by a linear polynomial. Since previous clinical studies have pointed out a close link between the repolarization response and the risk of suffering from arrhythmic death, we suggest that the proposed methodology can be applied to improve risk stratification, and in particular to assess the efficacy of treatment with antiarrhythmic drugs.

Acknowledgements

This study was supported by Ministerio de Ciencia y Tecnología and FEDER under Project TEC2004-05263-C02-02, in part by the Diputación General de Aragón (DGA), Spain, through Grupos Consolidados GTC ref: T30, and by CIBER through ISCIII CIBER CB06/01/0062.

Appendix A

For the linear state-space model described in Section 2.2.1 that has additive process and measurement noises, the following notations are introduced:

$\hat{\mathbf{m}}^-(n)$ and $\hat{\mathbf{m}}(n)$ are the a priori and a posteriori, respectively, state estimates at time n.
$\mathbf{e}^-(n)$ and $\mathbf{e}(n)$ are the a priori and a posteriori, respectively, estimate errors at time n:

$$\mathbf{e}^-(n) = \mathbf{m}(n) - \hat{\mathbf{m}}^-(n), \quad \mathbf{e}(n) = \mathbf{m}(n) - \hat{\mathbf{m}}(n).$$

$\mathbf{P}^-(n)$ and $\mathbf{P}(n)$ are the a priori and a posteriori, respectively, estimate error covariances at time n:

$$\mathbf{P}^-(n) = E\{\mathbf{e}^-(n)\,\mathbf{e}^-(n)^{\mathrm{T}}\}, \quad \mathbf{P}(n) = E\{\mathbf{e}(n)\,\mathbf{e}(n)^{\mathrm{T}}\}.$$

$\mathbf{K}(n)$ is the Kalman gain defined as $\mathbf{K}(n) = \mathbf{P}_{m\tilde{y}}(n)P_{\tilde{y}\tilde{y}}^{-1}(n)$, with

$$\begin{aligned}
\mathbf{P}_{m\tilde{y}}(n) &= E\{(\mathbf{m}(n) - \hat{\mathbf{m}}^-(n))(\tilde{\mathbf{y}}_{\mathrm{QT}}(n) - \hat{\tilde{\mathbf{y}}}_{\mathrm{QT}}^-(n))^{\mathrm{T}}\},\\
\mathbf{P}_{\tilde{y}\tilde{y}}(n) &= E\{(\tilde{\mathbf{y}}_{\mathrm{QT}}(n) - \hat{\tilde{\mathbf{y}}}_{\mathrm{QT}}^-(n))(\tilde{\mathbf{y}}_{\mathrm{QT}}(n) - \hat{\tilde{\mathbf{y}}}_{\mathrm{QT}}^-(n))^{\mathrm{T}}\},\\
\hat{\tilde{\mathbf{y}}}_{\mathrm{QT}}^-(n) &= \tilde{\mathbf{S}}^{\mathrm{T}}(n)\,\hat{\mathbf{m}}^-(n).
\end{aligned}$$

The equations of the **Kalman Filter** can be summarized as

(i) Initialize with:

$$\hat{\mathbf{m}}(0) = E\{\mathbf{m}(0)\} = \mu_{0,\mathbf{m}},$$

$$\mathbf{P}(0) = E\{(\mathbf{m}(0) - \hat{\mathbf{m}}(0))(\mathbf{m}(0) - \hat{\mathbf{m}}(0))^{\mathrm{T}}\} = \Pi_{0,\mathbf{m}}.$$

(ii) For $n = 0, 1, \ldots$, compute:
– Time-update:

$$\hat{\mathbf{m}}^-(n+1) = \hat{\mathbf{m}}(n), \quad \mathbf{P}^-(n+1) = \mathbf{P}(n) + \mathbf{Q}_{\mathbf{u}_{\mathbf{m}}}(n),$$

$$\hat{\tilde{\mathbf{y}}}_{\mathrm{QT}}^-(n+1) = \tilde{\mathbf{S}}^{\mathrm{T}}(n+1)\hat{\mathbf{m}}^-(n+1).$$

– Measurement-update

$$
\begin{aligned}
\mathbf{P}_{\tilde{y}\tilde{y}}(n+1) &= \tilde{\mathbf{S}}^{\mathrm{T}}(n+1)\,\mathbf{P}^{-}(n+1)\,\tilde{\mathbf{S}}(n+1) + \mathbf{R}_{\tilde{v}}(n+1),\\
\mathbf{P}_{m\tilde{y}}(n+1) &= \mathbf{P}^{-}(n+1)\,\tilde{\mathbf{S}}(n+1),\\
\mathbf{K}(n+1) &= \mathbf{P}_{m\tilde{y}}(n+1)\,\mathbf{P}_{\tilde{y}\tilde{y}}^{-1}(n+1), \quad \gamma^{-}(n+1) = \tilde{\mathbf{y}}_{\mathrm{QT}}(n+1) - \hat{\bar{\mathbf{y}}}_{\mathrm{QT}}^{-}(n+1),\\
\hat{\mathbf{m}}(n+1) &= \hat{\mathbf{m}}^{-}(n+1) + \mathbf{K}(n+1)\gamma^{-}(n+1),\\
\mathbf{P}(n+1) &= \mathbf{P}^{-}(n+1) - \mathbf{K}(n+1)\,\mathbf{P}_{\tilde{y}\tilde{y}}(n+1)\mathbf{K}^{T}(n+1).
\end{aligned}
$$

Appendix B

For the nonlinear state-space model described in Section 2.2.2 that has additive process and measurement noises, definitions of $\hat{\mathbf{c}}^{-}(n)$, $\hat{\mathbf{c}}(n)$, $\mathbf{e}^{-}(n)$, $\mathbf{e}(n)$, $\mathbf{P}^{-}(n)$, $\mathbf{P}(n)$ and $\mathbf{K}(n)$ are introduced that are analogous to those in Appendix A, except $\mathbf{m}(n)$ is replaced by $\mathbf{c}(n)$.

Equations of the **Unscented Kalman Filter** can be summarized as follows:

(i) Initialize with:

$$\hat{\mathbf{c}}(0) = E\{\mathbf{c}(0)\} = \boldsymbol{\mu}_{0,\mathbf{c}},$$

$$\mathbf{P}(0) = E\{(\mathbf{c}(0) - \hat{\mathbf{c}}(0))(\mathbf{c}(0) - \hat{\mathbf{c}}(0))^{\mathrm{T}}\} = \Pi_{0,\mathbf{c}}.$$

(ii) Define

α_{F} = positive scaling parameter indicative of the spread of the sigma points around the mean value of $\mathbf{c}(n)$.

β_{F} = non-negative weighting parameter used to incorporate prior knowledge of the distribution of $\mathbf{c}(n)$.

κ_{F} = secondary scaling parameter ≥ 0 to guarantee positive semidefiniteness of covariance matrices.

$\zeta = \alpha_{\mathrm{F}}^2(L_{\mathbf{c}} + \kappa_{\mathrm{F}}) - L_{\mathbf{c}}$. In this study, $\alpha_{\mathrm{F}} = 0.5$, $\beta_{\mathrm{F}} = 0$ and $\kappa_{\mathrm{F}} = 0$ are chosen.

Evaluate vectors $\mathbf{w}^{(m)}$ and $\mathbf{w}^{(c)}$, both of dimension $1 \times 2L_{\mathbf{c}}$, containing the following weighting factors to be used in the iterative procedure:

$$
\begin{aligned}
w_0^{(m)} &= \frac{\zeta}{L_{\mathbf{c}} + \zeta}, \quad w_0^{(c)} = \frac{\zeta}{L_{\mathbf{c}} + \zeta} + (1 - \alpha_{\mathrm{F}}^2 + \beta_{\mathrm{F}}),\\
w_j^{(m)} &= w_j^{(c)} = \frac{1}{2(L_{\mathbf{c}} + \zeta)}, \quad j = 1, 2, \ldots, 2L_{\mathbf{c}}.
\end{aligned}
$$

(iii) Compute for $n = 0, 1, \ldots$:

– Sigma points:

$$
\begin{aligned}
&\chi_0(n) = \hat{\mathbf{c}}(n), \quad \chi_j(n) = \hat{\mathbf{c}}(n) + \left(\sqrt{(L_{\mathbf{c}} + \zeta)\,\mathbf{P}(n)}\right)_j,\\
&j = 1, \ldots, L_{\mathbf{c}},\\
&\chi_j(n) = \hat{\mathbf{c}}(n) - \left(\sqrt{(L_{\mathbf{c}} + \zeta)\,\mathbf{P}(n)}\right)_{j-L_{\mathbf{c}}},\\
&j = L_{\mathbf{c}} + 1, \ldots, 2L_{\mathbf{c}},
\end{aligned}
$$

where $\left(\sqrt{(L_{\mathbf{c}} + \zeta)\mathbf{P}(n)}\right)_j$ denotes the j-th column of the matrix square root.

– Time-update

$$
\begin{aligned}
&\chi_j{}^{-}(n+1) = \chi_j(n), \quad j = 0, \ldots, 2L_{\mathrm{c}},\\
&\hat{c}^{-}(n+1) = \hat{c}(n), \qquad P^{-}(n+1) = P(n) + Q_{u_c}(n),\\
&\theta_j{}^{-}(n+1) = \bar{f}(x_{RR}(n),\ \chi_j{}^{-}(n+1)), \quad j = 0, \ldots, 2L_{\mathrm{c}},\\
&\hat{\bar{y}}_{\mathrm{QT}}{}^{-}(n+1) = \sum_{j=0}^{2L_{\mathrm{c}}} w_j{}^{(m)}\theta_j{}^{-}(n+1).
\end{aligned}
$$

– Measurement-update

$$
\begin{aligned}
\mathbf{P}_{\tilde{y}\tilde{y}}(n+1) &= \sum_{j=0}^{2L_{\mathbf{c}}} w_j^{(c)}(\theta_j^{-}(n+1) - \hat{\bar{\mathbf{y}}}_{\mathrm{QT}}^{-}(n+1))(\theta_j^{-}(n+1) - \hat{\bar{\mathbf{y}}}_{\mathrm{QT}}^{-}(n+1))^{\mathrm{T}} + \mathbf{R}_{\tilde{v}}(n+1),\\
\mathbf{P}_{c\tilde{y}}(n+1) &= \sum_{j=0}^{2L_{\mathbf{c}}} w_j^{(c)}(\chi_j^{-}(n+1) - \hat{\mathbf{c}}^{-}(n+1))(\theta_j^{-}(n+1) - \hat{\bar{\mathbf{y}}}_{\mathrm{QT}}^{-}(n+1))^{\mathrm{T}},\\
\mathbf{K}(n+1) &= \mathbf{P}_{c\tilde{y}}(n+1)\mathbf{P}_{\tilde{y}\tilde{y}}^{-1}(n+1), \quad \gamma^{-}(n+1) = \tilde{\mathbf{y}}_{\mathrm{QT}}(n+1) - \hat{\bar{\mathbf{y}}}_{\mathrm{QT}}^{-}(n+1),\\
\hat{\mathbf{c}}(n+1) &= \hat{\mathbf{c}}^{-}(n+1) + \mathbf{K}(n+1)\gamma^{-}(n+1),\\
\mathbf{P}(n+1) &= \mathbf{P}^{-}(n+1) - \mathbf{K}(n+1)\,\mathbf{P}_{\tilde{y}\tilde{y}}(n+1)\mathbf{K}(n+1)^{\mathrm{T}}.
\end{aligned}
$$

References

[1] A. Pathak, D. Curnier, J. Fourcade, J. Roncalli, P.K. Stein, P. Hermant, M. Bousquet, P. Massabuau, J.M. Senard, J.L. Montastruc, M. Galinier, QT dynamicity: a prognostic factor for sudden cardiac death in chronic heart failure, Eur. J. Heart Fail. 7 (2) (2005) 269–275.

[2] P. Chevalier, H. Burri, P. Adeleine, G. Kirkorian, M. Lopez, A. Leizorovicz, X. Andre-Fouet, P. Chapon, P. Rubel, P. Touboul, QT dynamicity and sudden death after myocardial infarction: results of a long-term follow-up study, J. Cardiovasc. Electrophysiol. 14 (3) (2003) 227–233.

[3] N.J. Linker, A.J. Camm, D.E. Ward, Dynamics of ventricular repolarisation in the congenital long QT syndromes, Br. Heart J. 66 (3) (1991) 230–237.

[4] F. Badilini, P. Maison-Blanche, R. Childers, P. Coumel, QT interval analysis on ambulatory electrocardiogram recordings: a selective beat averaging approach, Med. Biol. Eng. Comput. 37 (1999) 71–79.

[5] E. Pueyo, P. Smetana, P. Caminal, A.B. de Luna, M. Malik, P. Laguna, Characterization of QT interval adaptation to RR interval changes and its use as a risk-stratifier of arrhythmic mortality in amiodarone-treated

survivors of acute myocardial infarction, IEEE Trans. Biomed. Eng. 51 (9) (2004) 1511–1520.

[6] C.C. Lang, A.D. Flapan, J. Neilson, The impact of QT lag compensation on dynamic assessment of ventricular repolarization: reproducibility and the impact of lead selection, Pacing Clin. Electrophysiol. 24 (3) (2001) 366–373.

[7] S. Sala, G. Malfatto, E.H. Locati, G.M. DeFerrari, P.J. Schwartz, Diagnostic value of exercise-induced T wave abnormalities in the idiopathic long QT syndrome, Circulation 86 (1) (1992) I–392.

[8] L. Toivonen, K. Helenius, M. Viitasalo, Electrocardiographic repolarization during stress from awakening on alarm call, J. Am. Coll. Cardiol. 30 (3) (1997) 774–779.

[9] P. Langley, D. di Bernardo, A. Murray, Quantification of T wave shape changes following exercise, Pacing Clin. Electrophysiol. 25 (8) (2002) 1230–1234.

[10] D. di Bernado, A. Murray, Computer model for study of cardiac repolarization, J. Cardiovasc. Electrophysiol. 11 (2000) 895–899.

[11] S. Haykin, Adaptive Filter Theory, Prentice Hall, Upper Saddle River, NJ, 2002.

[12] A. Voutilainen, J. Kaipio, Estimation of non-stationary aerosol size distributions using the state space approach, J. Aerosol. Sci. 32 (2001) 631–648.

[13] G.H. Golub, P.C. Hansen, D.P. O'Leary, Tikhonov regularization and total least squares, SIAM J. Matrix Anal. Appl. 21 (1) (1999) 185–194.

[14] Y. Yang, H. Lev-Ari, Identification of Linear Time-Variant Systems without using Prior Information, in: Proceedings of IEEE Conference on Acoustics, Speech and Signal Processing, 2002, pp. 1741–1744.

[15] D. Simon, D.L. Simon, Aircraft turbofan engine health estimation using constrained Kalman Filtering, SME J. Eng. Gas Turb. Power 127 (2) (2005) 323–328.

[16] A. Voutilainen, Statistical Inversion Methods for the Reconstruction of Aerosol Size Distributions, University of Kuopio, 2001.

[17] S.J. Julier, J.K. Uhlmann, A new extension of the Kalman Filter to nonlinear systems, in: Proceedings of AeroSense: The 11th International Symposium on Aerospace/Defence Sensing, Simulation and Controls, Multi Sensor Fusion, Tracking and Resource Management II, SPIE, 1997.

[18] S.J. Julier, J.K. Uhlmann, Unscented filtering and nonlinear estimation, in: Proceedings of the IEEE, vol. 92, no. 3, 2004, pp. 401–422.

[19] J. Martinez, R. Almeida, S. Olmos, A. Rocha, P. Laguna, A Wavelet-based ECG delineator: evaluation on standard databases, IEEE Trans. Biomed. Eng. 51 (4) (2004) 570–581.

[20] F. Hampel, E. Ronchetti, P. Rousseeuw, W. Stahel, Robust Statistics, John Wiley and Sons, New York, USA, 1986.

[22] V.N. Batchvarov, A. Ghuran, P. Smetana, K. Hnatkova, M. Harries, P. Dilaveris, A.J. Camm, M. Malik, QT-RR relationship in healthy subjects exhibits substantial intersubject variability and high intrasubject stability, Am. J. Physiol. Heart Circ. Physiol. 282 (6) (2002) 2356–2363.

[23] C.P. Lau, A.R. Freedman, S. Flemming, M. Malik, A.J. Camm, D.E. Ward, Hysteresis of the ventricular paced QT interval in response to abrupt changes in pacing rate, Cardiovasc. Res. 22 (2) (1988) 67–72.